Adaptive Robust Control of an Omnidirectional Mobile Platform for Autonomous Service Robots in Polar Coordinates

Hsu-Chih Huang · Ching-Chih Tsai

Abstract This paper presents an adaptive robust control method for trajectory tracking and path following of an omni-directional wheeled mobile platform with actuators' uncertainties. The polar-space kinematic model of the platform with three independent driving omnidirectional wheels equally spaced at 120 from one another is briefly introduced, and the dynamic models of the three uncertain servomotors mounted on the driving wheels are also described. With the platform's kinematic model and the motors' dynamic model associated two unknown parameters, the adaptive robust controller is synthesized via the integral backstepping approach. Computer simulations and experimental results are conducted to show the effectiveness and merits of the proposed control method in comparison with a conventional PI feedback control method.

Keywords Adaptive control · Backstepping · Omnidirectional mobile platform · Robust control

1 Introduction

Recently, omni-directional mobile platforms have attracted much attention in the robotics as well as control societies. Such platforms have been extensively used for the well-known RoboCup competition in order to have manoeuvring movements. Moreover, this type of platform has also been shown very suitable for material handling. In comparison with conventional two-wheeled or four wheeled ("car-like") mobile platforms [1, 2, 4, 7, 9, 10, 14, 15, 21], omni-directional mobile platforms have an agile ability to move toward any direction and to simultaneously attain desired orientation, namely that they do not have

H.-C. Huang · C.-C. Tsai (✉)
Department of Electrical Engineering, National Chung Hsing University, 250, Kuo-Kuang Road, Taichung 402, Taiwan
e-mail: cctsai@dragon.nchu.edu.tw

so-called nonholonomic constraints. This manoeuvring capability is particularly useful in designing mobile platforms for autonomous service robots, such as home-care robot, nursing-care robots, medical robots, mobile manipulators and so on.

Omni-directional mobile platforms and their controls have been investigated by several researchers. Pin et al. [16] presented the concepts for a family of holonomic wheeled platforms that feature full omnidirectionality with simultaneous and independently controlled and translational capabilities. Jung et al. [11] constructed a kind of omnidirectional base, derived its kinematical and dynamic models, and then presented a fuzzy controller to steer the robot. Carter et al. [3] introduced the mechanical design process and independent PID wheel controllers for their own omnidirectional mobile platform used as the Ohio University RoboCup team player. Kalmár-Nagy et al. [12] in Cornell University proposed a method of generating near-optimal trajectories for an omnidirectional robot; this method provided an efficient method of path planning and allowed a large number of possible scenarios to be explored in real time. Watanabe et al. [19] presented a PI feedback control method for an omnidirectional mobile platform which is equipped with three lateral orthogonal-wheel assemblies. William II et al. [20] presented a dynamic model for omnidirectional wheeled mobile platforms, considering the occurrence of slip between the wheels and motion surface. With the dynamic model from [3], Tsai et al. [18] proposed the simultaneous point stabilization and trajectory tracking method via backstepping; this method did not consider the issues of the parameter variations and the uncertainties from friction and slip. Yang and Red [23] constructed an on-line Cartesian trajectory control of mechanism along complex curves and Red [17] presented a dynamic optimal trajectory generator for Cartesian path following; however, they did not cope with polar-space control problems.

Polar space is especially useful in situations where the relationship between two points is most easily expressed in terms of angle and distance. There are many simple polar-space equations which describe complex curves, for example, the rose curves and the Limacon of Pascal. The path following and trajectory tracking problems for nonholonomic mobile platforms in polar space have been investigated by several researchers. Aicardi et al. [1] presented the closed loop steering of unicycle-like vehicles via Lyapunov techniques. Point stabilization of mobile platforms via state-space exact feedback linearization was developed by Park et al. [15]. Yang and Kim [22] presented the sliding mode control for trajectory tracking of nonholonomic wheeled mobile platforms. Chwa [4] presented the polar-space sliding-mode tracking controller to steer a nonholonomic wheeled mobile platform incorporating its dynamic effects and external disturbances; the controller was shown effective to have fast response, good transient performance and robustness with regard to parameter variations. Many of the earlier works addressing the tracking problem were described in [5, 6, 8]. However, as the authors' best understanding, the trajectory tracking and path following problems of an omnidirectional mobile platform in polar coordinates remains open. Although it is argued that for an omnidirectional platform there is no need to consider polar model due to the fact that the model is not defined at the origin, we believe that the polar model can be used to design effective controllers for the trajectory tracking and path following problems in polar coordinates.

The goal of this paper is to put emphasis on using the adaptive backstepping approach [7, 13] to construct a unified controller to achieve trajectory tracking and path following for an omnidirectional platform incorporating with two motors' uncertainties. The proposed controller will be proven with the property of globally exponential stability. Computer simulations are performed on an omnidirectional mobile platform with three independent

driving wheels equally space at 120 degrees from one another. The developed control method, assuming that the position and orientation of the platform be directly measured, is particularly useful in developing a home-care or nursing-care omnidirectional mobile robot or manipulator. Overall, the contributions of the paper are threefold.

1. A novel polar-space robust controller is presented for omnidirectional mobile platforms with uncertainties for tracking the special curves that are not easily expressed in Cartesian coordinates.
2. A new adaptive control scheme for Part 1 is proposed. Simulation and experimental results are illustrated to examine the performance of the polar-space adaptive robust controller.
3. The proposed adaptive robust controller is straightforward extended to address the path following problem in order to exactly follow time-independent polar-space path.

The rest of this paper is organized as follows. In Section 2, the kinematic model of the omni-directional wheeled mobile platform with its motors' dynamics and uncertainties is briefly presented in polar-coordinates. Section 3 synthesizes an adaptive robust controller via the adaptive backstepping approach. In Section 4, the adaptive controller is applied to address the path following problem. Section 5 conducts several simulations that are used for illustration of the merits of the proposed control methods. Section 6 presents two experimental results for elliptical path tracking and Limacon of Pascal path following. Section 7 concludes the paper.

2 Platform's Polar-space Kinematic Model and Motors' Models with Uncertainties

2.1 Brief Description of the Platform's Kinematic Model in Polar Coordinates

This section is devoted to briefly describing the polar-space kinematic model of an omnidirectional mobile platform with three independent omnidirectional wheels equally spaced at 120° from one another. Figure 1 depicts its structure and geometry that is used to find the polar-space kinematic model of the platform, where θ denotes the vehicle orientation. Due to structural symmetry, the vehicle has the property that the center of geometry coincides with the center of mass.
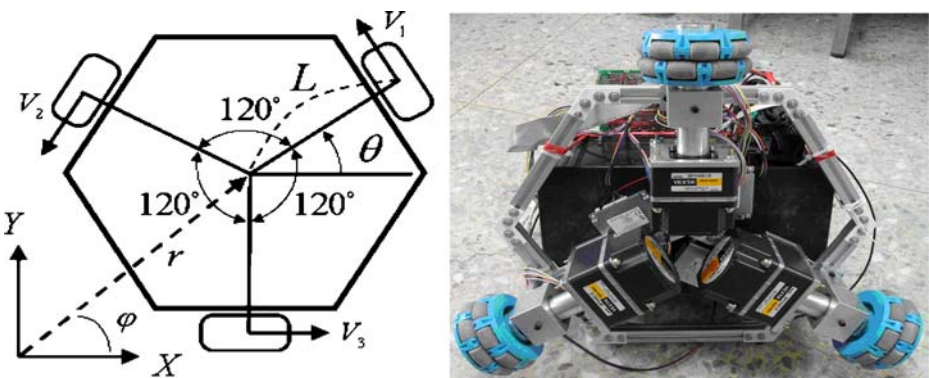

Fig. 1 Structure and geometry of the omnidirectional mobile platform in polar coordinates

Before deriving the polar-space kinematic model, let us define the pose of the platform as $[x(t)\ y(t)\ \theta(t)]^{\mathrm{T}}$, assume that no slips occur, and recall that the platform's kinematic equations in Cartesian space is given by

$$\begin{bmatrix} V_1(t) \\ V_2(t) \\ V_3(t) \end{bmatrix} = \begin{bmatrix} R\omega_1(t) \\ R\omega_2(t) \\ R\omega_3(t) \end{bmatrix} = P(\theta(t)) \begin{bmatrix} \dot{x}(t) \\ \dot{y}(t) \\ \dot{\theta}(t) \end{bmatrix} \tag{1}$$

or

$$\begin{bmatrix} \dot{x}(t) \\ \dot{y}(t) \\ \dot{\theta}(t) \end{bmatrix} = P^{-1}(\theta(t)) \begin{bmatrix} R\omega_1(t) \\ R\omega_2(t) \\ R\omega_3(t) \end{bmatrix} = P^{-1}(\theta(t)) \begin{bmatrix} V_1(t) \\ V_2(t) \\ V_3(t) \end{bmatrix} \tag{2}$$

where

$$P(\theta(t)) = \begin{bmatrix} -\sin\theta(t) & \cos\theta(t) & L \\ -\sin\left(\frac{\pi}{3}-\theta(t)\right) & -\cos\left(\frac{\pi}{3}-\theta(t)\right) & L \\ \sin\left(\frac{\pi}{3}+\theta(t)\right) & -\cos\left(\frac{\pi}{3}+\theta(t)\right) & L \end{bmatrix} \quad \text{and}$$

$$P^{-1}(\theta(t)) = \begin{bmatrix} -\frac{2}{3}\sin\theta(t) & -\frac{2}{3}\sin\left(\frac{\pi}{3}-\theta(t)\right) & \frac{2}{3}\sin\left(\frac{\pi}{3}+\theta(t)\right) \\ \frac{2}{3}\cos\theta(t) & -\frac{2}{3}\cos\left(\frac{\pi}{3}-\theta(t)\right) & -\frac{2}{3}\cos\left(\frac{\pi}{3}+\theta(t)\right) \\ \frac{1}{3L} & \frac{1}{3L} & \frac{1}{3L} \end{bmatrix}$$

and R denotes the radius of the driving wheels, and $V_i(t)$ and $\omega_i(t)$, $i=1, 2, 3$, respectively denote the linear and angular velocities of each wheel.

To express the model (2) in polar coordinates, we have

$$r(t) = \sqrt{x^2(t) + y^2(t)}, x(t) = r(t)\cos\varphi(t), y(t) = r(t)\sin\varphi(t) \tag{3}$$

where, as Fig. 1 shows, r denotes the polar radius, and φ represents the polar angle. With the time derivative of Eq. 3

$$\begin{aligned} \dot{r}(t) &= \frac{x(t)\dot{x}(t)+y(t)\dot{y}(t)}{\sqrt{x^2(t)+y^2(t)}} = \frac{x(t)\dot{x}(t)+y(t)\dot{y}(t)}{r(t)} \\ \dot{x}(t) &= \dot{r}(t)\cos\varphi(t) - r(t)\,\dot{\varphi}(t)\sin\varphi(t) \\ \dot{y}(t) &= \dot{r}(t)\sin\varphi(t) + r(t)\,\dot{\varphi}(t)\cos\varphi(t) \end{aligned} \tag{4}$$

one can combine Eqs. 2, 3 and 4 to obtain the kinematic model of the platform in polar coordinates. Thus, it follows from Eq. 4 that the time derivative of the polar radius is given by

$$\begin{aligned} \dot{r}(t) &= \frac{x(t)\dot{x}(t) + y(t)\dot{y}(t)}{r(t)} = \frac{\dot{x}(t)r(t)\cos\varphi(t) + \dot{y}(t)r(t)\sin\varphi(t)}{r(t)} \\ &= \dot{x}(t)\cos\varphi(t) + \dot{y}(t)\sin\varphi(t) \\ &= \begin{bmatrix} -\frac{2}{3}\sin(\theta(t)-\varphi(t)) & -\frac{2}{3}\sin\left(\frac{\pi}{3}-(\theta(t)-\varphi(t))\right) & \frac{2}{3}\sin\left(\frac{\pi}{3}+\theta(t)-\varphi(t)\right) \end{bmatrix} \begin{bmatrix} R\omega_1(t) \\ R\omega_2(t) \\ R\omega_3(t) \end{bmatrix} \end{aligned} \tag{5}$$

Using the equality

$$\dot{y}(t)\cos\varphi(t) - \dot{x}(t)\sin\varphi(t) = r(t)\left(\sin^2\varphi(t) + \cos^2\varphi(t)\right)\dot{\varphi}(t) = r(t)\,\dot{\varphi}(t)$$

and Eq. 4 yields

$$
\begin{aligned}
\dot{\varphi}(t) &= \frac{1}{r(t)}\left(\dot{y}(t)\cos\varphi(t) - \dot{x}(t)\sin\varphi(t)\right)\\
&= \frac{1}{r(t)}\left[\frac{2}{3}\cos\left(\theta(t) - \varphi(t)\right) \quad -\frac{2}{3}\cos\left(\frac{\pi}{3} - (\theta(t) - \varphi(t))\right)\right.\\
&\qquad \left. -\frac{2}{3}\cos\left(\frac{\pi}{3} + \theta(t) - \varphi(t)\right)\right]
\begin{bmatrix} R\omega_1(t)\\ R\omega_2(t)\\ R\omega_3(t) \end{bmatrix}
\end{aligned}
\tag{6}
$$

Moreover, from Eq. 2, it is easy to obtain

$$\dot{\theta}(t) = \begin{bmatrix} \dfrac{1}{3L} & \dfrac{1}{3L} & \dfrac{1}{3L} \end{bmatrix}
\begin{bmatrix} R\omega_1(t)\\ R\omega_2(t)\\ R\omega_3(t) \end{bmatrix}
\tag{7}$$

Combining Eqs. 5, 6 and 7 gives the kinematical model of the omnidirectional mobile platform in polar coordinates as follows;

$$\begin{bmatrix} \dot{r}(t)\\ \dot{\varphi}(t)\\ \dot{\theta}(t) \end{bmatrix} = T^{-1}(r(t),\theta(t) - \varphi(t))
\begin{bmatrix} R\omega_1(t)\\ R\omega_2(t)\\ R\omega_3(t) \end{bmatrix}
\tag{8}$$

where

$$T^{-1}(r(t),\theta(t) - \varphi(t))$$

$$= \begin{bmatrix}
-\frac{2}{3}\sin\left(\theta(t) - \varphi(t)\right) & -\frac{2}{3}\sin\left(\frac{\pi}{3} - (\theta(t) - \varphi(t))\right) & \frac{2}{3}\sin\left(\frac{\pi}{3} + \theta(t) - \varphi(t)\right)\\
\frac{2}{3r(t)}\cos\left(\theta(t) - \varphi(t)\right) & -\frac{2}{3r(t)}\cos\left(\frac{\pi}{3} - (\theta(t) - \varphi(t))\right) & -\frac{2}{3r(t)}\cos\left(\frac{\pi}{3} + \theta(t) - \varphi(t)\right)\\
\frac{1}{3L} & \frac{1}{3L} & \frac{1}{3L}
\end{bmatrix}$$

Note that the model (8) is undefined for zero polar radius; the model is valid for the condition $r(t) > \varepsilon$ where ε is an arbitrarily small and positive real number. Furthermore, the matrix $T^{-1}(r(t), \theta(t) - \varphi(t))$ is nonsingular for nonzero polar radius and the inversion of the matrix $T^{-1}(r(t), \theta(t) - \varphi(t))$ for $r(t) \neq 0$ can be found as below;

$$T(r(t),\theta(t) - \varphi(t)) = \begin{bmatrix}
-\sin\left(\theta(t) - \varphi(t)\right) & r(t)\cos\left(\theta(t) - \varphi(t)\right) & L\\
-\sin\left(\frac{\pi}{3} - (\theta(t) - \varphi(t))\right) & -r(t)\cos\left(\frac{\pi}{3} - (\theta(t) - \varphi(t))\right) & L\\
\sin\left(\frac{\pi}{3} + (\theta(t) - \varphi(t))\right) & -r(t)\cos\left(\frac{\pi}{3} + (\theta(t) - \varphi(t))\right) & L
\end{bmatrix}
\tag{9}$$

2.2 Motors' Dynamic Models with Two Unknown Parameters

In order to derive the dynamic models for the three servomotors mounted on the driving wheels, one assumes that the three same servomotors have two unknown but constant parameters, the moment of inertia J and the viscous coefficient B, and three exogenous, uncertain but bounded torques, $Td_i(t)$, $i=1, 2, 3$, exerted on the driving wheels. The

assumption of unknown but constant parameters, J and B, is relevant not only at the modeling process, but also during operation for mission execution in case of payload changes. The bounded exogenous torque $Td_i(t)$ may be caused by several factors, such as the static friction between the wheel and the surface, and the slip phenomena where the force may vary with the surface made by the used materials. Note that $|Td_i| \leq Td_{i\max}$.

With the torque generated by each DC servomotor motor and the bounded exogenous torque Td_i exerted on each wheel, the dynamic equations of each model with negligible motor inductance are obtained from Newton's second law for rotation,

$$
\begin{aligned}
U_i(t) &= R_a I_i(t) + k_e r_g \omega_i(t) \\
T_i(t) &= k_t I_i(t) = J r_g \dot{\omega}_i(t) + B r_g \omega_i(t) + T d_i(t)
\end{aligned}
\tag{10}
$$

where $U_i(t)$, $i=1, 2, 3$, is the applied voltage of each motor; $\omega_i(t)$, $i=1, 2, 3$, respectively denote the angular velocities of each wheel; R_a is the armature resistance of the servomotors; B is the viscous coefficient; r_g is the gear ratio; k_e denotes the back-emf coefficient; k_t represents the torque coefficient; $T_i(t)$ is the electromagnetic torque. Note that these parameters R_a, k_e and k_t can be obtained from the motors' data sheets provided by the vender. With the force (2), one obtains the dynamics of the three servomotors in the vector-matrix

$$
\begin{bmatrix} \dot{\omega}_1(t) \\ \dot{\omega}_2(t) \\ \dot{\omega}_3(t) \end{bmatrix} = \alpha \begin{bmatrix} U_1(t) \\ U_2(t) \\ U_3(t) \end{bmatrix} - \beta \begin{bmatrix} \omega_1(t) \\ \omega_2(t) \\ \omega_3(t) \end{bmatrix} - \begin{bmatrix} f_1(t) \\ f_2(t) \\ f_3(t) \end{bmatrix} = \alpha U(t) - \beta \omega(t) - f(t), \alpha > 0, \beta > 0
\tag{11}
$$

w h e r e $U(t) = [U_1(t) \quad U_2(t) \quad U_3(t)]^T$; $\omega(t) = [\omega_1(t) \quad \omega_2(t) \quad \omega_3(t)]^T$; $\alpha = \frac{k_t}{JR_a r_g}$; $\beta = \frac{k_e k_t + B}{JR_a}$; $f(t) = [f_1(t) \quad f_2(t) \quad f_3(t)]^T$.
where $f_i(t) = \frac{Td_i(t)}{Jr_g}$, $i=1, 2, 3$. Note that the two parameters α and β are assumed constant but unknown, and the uncertain and exogenous torque vector satisfies the inequality $\|f\|_\infty \leq f_{\max}$ since $|Td_i| \leq Td_{i\max}$.

3 Adaptive Robust Trajectory Tracking

This section synthesizes an adaptive robust controller for the platform associated with the kinematic model (8) and the motors' dynamic model (11) via integral backstepping. This controller aims at steering the platform to reach the destination pose or exactly follow desired trajectory with maneuvering capability. In order to solve for the adaptive robust control problem, the desired and differentiable trajectory is described by $[r_d(t) \quad \varphi_d(t) \quad \theta_d(t)]^T \in C^1$. Note that if the desired trajectory is independent of time, that is, a fixed destination pose, then the control problem is referred to the so-called regulation problem; otherwise, the control problem is the so-called trajectory tracking. Unlike conventional two-wheeled or four-wheeled (car-like) mobile platforms, the desired trajectory can not be generated from the platform's kinematics, but can be any smooth but differentiable time function. In the following we elucidate how to use the backstepping approach to synthesize the adaptive robust controller step by step.

3.1 Step 1: Robust Controller Design

This step is dedicated to deriving a nonlinear controller to achieve trajectory tracking under the conditions of no unknown parameters. Unlike the wheeled mobile platforms with

differential driving configuration, the polar-coordinate control rule for the omnidirectional mobile platforms with the kinematic model (8) can be rather easily developed. In what follows the kinematic controller is first designed and the complete robust controller is then synthesized via the integral backstepping approach.

To design the controller, one defines the pose tracking error

$$
Z_e(t) = \begin{bmatrix} r_e(t) \\ \varphi_e(t) \\ \theta_e(t) \end{bmatrix} = \begin{bmatrix} r(t) \\ \varphi(t) \\ \theta(t) \end{bmatrix} - \begin{bmatrix} r_d(t) \\ \varphi_d(t) \\ \theta_d(t) \end{bmatrix} \tag{12}
$$

which gives

$$
\begin{bmatrix} \dot{r}_e(t) \\ \dot{\varphi}_e(t) \\ \dot{\theta}_e(t) \end{bmatrix} = \begin{bmatrix} \dot{r}(t) \\ \dot{\varphi}(t) \\ \dot{\theta}(t) \end{bmatrix} - \begin{bmatrix} \dot{r}_d(t) \\ \dot{\varphi}_d(t) \\ \dot{\theta}_d(t) \end{bmatrix} = T^{-1}(r(t), \theta(t) - \varphi(t)) \begin{bmatrix} R\omega_1(t) \\ R\omega_2(t) \\ R\omega_3(t) \end{bmatrix} - \begin{bmatrix} \dot{r}_d(t) \\ \dot{\varphi}_d(t) \\ \dot{\theta}_d(t) \end{bmatrix} \tag{13}
$$

To stabilize the system, we propose the nonlinear control law (Eq. 14) where the matrix K_p is symmetric and positive definite.

$$
\begin{bmatrix} \omega_1^*(t) \\ \omega_2^*(t) \\ \omega_3^*(t) \end{bmatrix} = \frac{1}{R} T(r(t), \theta(t) - \varphi(t)) \left(-K_p \begin{bmatrix} r_e(t) \\ \varphi_e(t) \\ \theta_e(t) \end{bmatrix} + \begin{bmatrix} \dot{r}_d(t) \\ \dot{\varphi}_d(t) \\ \dot{\theta}_d(t) \end{bmatrix} \right), \quad K_p = K_p^T > 0 \tag{14}
$$

Taking Eq. 14 into Eq. 13, the dynamics of the closed-loop error system becomes

$$
\begin{bmatrix} \dot{r}_e(t) \\ \dot{\varphi}_e(t) \\ \dot{\theta}_e(t) \end{bmatrix} = T^{-1}(r(t), \theta(t) - \varphi(t)) T(r(t), \theta(t) - \varphi(t)) \tag{15}
$$

$$
\left(-K_p \begin{bmatrix} r_e(t) \\ \varphi_e(t) \\ \theta_e(t) \end{bmatrix} + \begin{bmatrix} \dot{r}_d(t) \\ \dot{\varphi}_d(t) \\ \dot{\theta}_d(t) \end{bmatrix} \right) - \begin{bmatrix} \dot{r}_d(t) \\ \dot{\varphi}_d(t) \\ \dot{\theta}_d(t) \end{bmatrix}
$$

$$
= -K_p \begin{bmatrix} r_e(t) \\ \varphi_e(t) \\ \theta_e(t) \end{bmatrix} + \begin{bmatrix} \dot{r}_d(t) \\ \dot{\varphi}_d(t) \\ \dot{\theta}_d(t) \end{bmatrix} - \begin{bmatrix} \dot{r}_d(t) \\ \dot{\varphi}_d(t) \\ \dot{\theta}_d(t) \end{bmatrix} = -K_p \begin{bmatrix} r_e(t) \\ \varphi_e(t) \\ \theta_e(t) \end{bmatrix}
$$

where the globally asymptotical stability of the closed-loop error system can be easily proven by selecting the quadratic Lyapunov function

$$
V_1(t) = \frac{1}{2} [r_e(t) \quad \varphi_e(t) \quad \theta_e(t)] \begin{bmatrix} r_e(t) \\ \varphi_e(t) \\ \theta_e(t) \end{bmatrix} \tag{16}
$$

Taking the time derivative of $V_1(t)$ along the trajectory of Eq. 13 obtains

$$
\dot{V}_1(t) = [r_e(t) \quad \varphi_e(t) \quad \theta_e(t)] \begin{bmatrix} \dot{r}_e(t) \\ \dot{\varphi}_e(t) \\ \dot{\theta}_e(t) \end{bmatrix} = [r_e(t) \quad \varphi_e(t) \quad \theta_e(t)] \left(-K_p \begin{bmatrix} r_e(t) \\ \varphi_e(t) \\ \theta_e(t) \end{bmatrix} \right)
$$

$$
= -[r_e(t) \quad \varphi_e(t) \quad \theta_e(t)] K_p \begin{bmatrix} r_e(t) \\ \varphi_e(t) \\ \theta_e(t) \end{bmatrix} < 0
$$

(17)

Since $\dot{V}_1(t)$ is negative definite, Lyapunov stability theory implies that $[r_e(t) \quad \varphi_e(t) \quad \theta_e(t)]^T \to [0 \quad 0 \quad 0]^T$ as $t \to \infty$. Moreover, it is easily shown that the origin, $[0\ 0\ 0]^T$, is globally exponential stable, that is, the position and orientation errors exponentially approach zero as time tends to infinity.

Next we move to find the motors' control voltage vector $U(t) = [U_1(t)\ U_2(t)\ U_3(t)]^T$ such that the actual angular velocity vector $\omega(t) = [\omega_1(t)\ \omega_2(t)\ \omega_3(t)]^T$ of the three motors is consistent with the desired velocity vector $\omega^*(t) = [\omega_1^*(t)\ \omega_2^*(t)\ \omega_3^*(t)]^T$ presented in Eq. 14. With the motors' model (11), this can be done easily via the well-known integral backstepping approach.

To achieve the goal, we define the following backstepping error vectors by

$$
\eta(t) = T^{-1}(r(t), \theta(t) - \varphi(t))(\omega(t) - \omega^*(t)) = T^{-1}(r(t), \theta(t) - \varphi(t))\widetilde{\omega}(t) \quad (18)
$$

where $\widetilde{\omega}(t) = \omega(t) - \omega^*(t)$. Taking the time derivative of the error vector $\eta(t)$

$$
\begin{aligned}
\dot{\eta}(t) &= \dot{T}^{-1}(r(t), \theta(t) - \varphi(t))\widetilde{\omega}(t) + T^{-1}(r(t), \theta(t) - \varphi(t))\dot{\widetilde{\omega}}(t) \\
&= \dot{T}^{-1}(r(t), \theta(t) - \varphi(t))\widetilde{\omega}(t) + T^{-1}(r(t), \theta(t) - \varphi(t)) \\
&\quad \left(\alpha U(t) - \beta(\widetilde{\omega}(t) + \omega^*(t)) - f(t) - \dot{\omega}^*(t) \right) \\
&= -\beta\eta(t) + \dot{T}^{-1}(r(t), \theta(t) - \varphi(t))\widetilde{\omega}(t) + T^{-1}(r(t), \theta(t) - \varphi(t)) \\
&\quad \left(\alpha U(t) - \beta\omega^*(t) - f(t) - \dot{\omega}^*(t) \right)
\end{aligned}
$$

(19)

To stabilize the dynamic equation 19, the subsequent control law is proposed

$$
U(t) = \alpha^{-1}\beta\omega^*(t) + \alpha^{-1}\dot{\omega}^*(t) - \alpha^{-1}T(r(t), \theta(t) - \varphi(t)) \quad (20)
$$

$$
\left[\dot{T}^{-1}(r(t), \theta(t) - \varphi(t))\widetilde{\omega}(t) + RZ_e(t) \right]
$$

$$
- T(r(t), \theta(t) - \varphi(t))[k_1\eta(t) + k_2\mathrm{sgn}(\eta(t))]
$$

where the gain k_1 and k_2 can be selected by the user such that the closed-loop error system can quickly decay to zero exponentially; $\mathrm{sgn}(.)$ denote the signum function. Substituting Eq. 20 into Eq. 19 yields

$$
\dot{\eta}(t) = -(\beta + \alpha k_1)\eta(t) - RZ_e(t) - \alpha k_2\mathrm{sgn}(\eta(t)) - T^{-1}(r(t), \theta(t) - \varphi(t))[f(t)], \quad (21)
$$

$$
k_1 > 0, k_2 > 0
$$

With the defined backstepping error vector, Eq. 13 is rewritten as

$$
\begin{bmatrix} \dot{r}_e(t) \\ \dot{\varphi}_e(t) \\ \dot{\theta}_e(t) \end{bmatrix} = T^{-1}(r(t), \theta(t) - \varphi(t)) \begin{bmatrix} R(\omega_1^*(t) + \tilde{\omega}_1(t)) \\ R(\omega_2^*(t) + \tilde{\omega}_2(t)) \\ R(\omega_3^*(t) + \tilde{\omega}_3(t)) \end{bmatrix} - \begin{bmatrix} \dot{r}_d(t) \\ \dot{\varphi}_d(t) \\ \dot{\theta}_d(t) \end{bmatrix} = -K_P \begin{bmatrix} r_e(t) \\ \varphi_e(t) \\ \theta_e(t) \end{bmatrix} + R\eta(t)
$$

(22)

For the asymptotical stability of the overall closed-loop error system (21) an (22), a radially unbounded Lyapunov function candidate is chosen as follows:

$$
V_2(t) = \frac{1}{2}[r_e(t) \quad \varphi_e(t) \quad \theta_e(t)] \begin{bmatrix} r_e(t) \\ \varphi_e(t) \\ \theta_e(t) \end{bmatrix} + \frac{1}{2}\eta^T(t)\eta(t)
$$

(23)

which leads to the time derivative of $V_2(t)$ along the trajectories of Eqs. 21 and 22

$$
\dot{V}_2(t) = [r_e(t) \quad \varphi_e(t) \quad \theta_e(t)] \begin{bmatrix} \dot{r}_e(t) \\ \dot{\varphi}_e(t) \\ \dot{\theta}_e(t) \end{bmatrix} + \eta^T(t)\dot{\eta}(t)
$$

(24)

$$
= Z_e^T(t)\left(-K_p Z_e(t) + R\eta(t)\right) + \eta^T(t)[-(\beta + \alpha k_1)\eta(t) - \alpha k_2 \text{sgn}(\eta(t)) - RZ_e(t)]
$$

$$
- \eta^T(t) T^{-1}(r(t), \theta(t) - \varphi(t))[f(t)]
$$

$$
= -Z_e^T K_p Z_e(t) - (\beta + \alpha k_1)\eta^T(t)\eta(t)
$$

$$
- \alpha k_2 \|\eta(t)\|_1 - \eta^T(t) T^{-1}(r(t), \theta(t) - \varphi(t))f(t)
$$

Using the inequalities $\left\|T^{-1}(r(t), \theta(t) - \varphi(t))f(t)\right\|_\infty \le k_{max}$ for any bounded and nonzero trajectory and, $k_2 \ge k_{max}/\alpha$, one obtains

$$
\dot{V}_2(t) \le -Z_e^T K_p Z_e(t) - (\beta + \alpha k_1)\eta^T(t)\eta(t)
$$

(25)

$$
- \alpha k_2 \|\eta(t)\|_1 + \|\eta(t)\|_1 \left\|T^{-1}(r(t), \theta(t) - \varphi(t))f(t)\right\|_\infty
$$

$$
\le -Z_e^T K_p Z_e(t) - (\beta + k_1)\eta^T(t)\eta(t) - \alpha\left(k_2 - \frac{k_{max}}{\alpha}\right)\|\eta(t)\|_1 \le 0
$$

which indicates that $\dot{V}_2(t)$ is negative semidefinite and $V_2(t)$ is indeed a Lyapunov equation. The use of the Lyapunov stability theory implies that $Z_e(t) \rightarrow [0\ 0\ 0]^T$ and $\eta(t) \rightarrow 0$ as $t \rightarrow \infty$. The fact that $\eta(t) \rightarrow 0$ as $t \rightarrow \infty$ indicates that $\tilde{\omega}(t) \rightarrow 0$ as $t \rightarrow \infty$ because $T^{-1}(r(t), \theta(t) - \varphi(t))$ is always nonsingular for any nonzero polar radius. The following theorem summarizes this subsection.

Theorem 1 *For the platform's kinematic model (8) along with the motors' dynamic model (11) and the control law (20), the platform can be steered to reach any destination pose or exactly track any smooth and differentiable trajectory in the sense of globally exponential stability, i.e., $r(t) \rightarrow r_d(t)$, $\varphi(t) \rightarrow \varphi_d(t)$ and $\theta(t) \rightarrow \theta_d(t)$ as $t \rightarrow \infty$.*

3.2 Step 2: Adaptive Robust Controller Design

This step aims to develop an adaptive robust control for the kinematic model (8) with the motors' dynamic model (11) under the assumption that the platform has two unknown but constant parameters, α and β, as well as three uncertain but bounded forces, f_i, $i=1$, 2, 3, exerted on the driving wheels. The reason why the two parameters, α and β, are supposed unknown but constant is that they depend upon the uncertain moment of inertia J which is caused by the abrupt load changes of the platform, and the unknown viscous coefficient B.

To circumvent possible performance degradation caused by these two unknown but constant parameters, we propose the following adaptive control law

$$U(t) = \hat{\alpha}^{-1}\hat{\beta}\omega^*(t) + \hat{\alpha}^{-1}\dot{\omega}^*(t) - \hat{\alpha}^{-1}T(r(t),\theta(t) - \varphi(t)) \tag{26}$$
$$\left[RZ_e(t) + T^{-1}(r(t),\theta(t) - \varphi(t))\tilde{\omega}(t) \right] - T(r(t),\theta(t) - \varphi(t))$$
$$[k_1\eta(t) + k_2\mathrm{sgn}(\eta(t))]$$

where $\hat{\alpha}$ and $\hat{\beta}$ are the estimates of α and β, respectively, and their parameter adjustment rules are to be determined in the following. Substituting Eq. 26 into 19 gives

$$\dot{\eta}(t) = -\beta\eta(t) + \left(\frac{\hat{\alpha} - \alpha}{\hat{\alpha}}\right) T^{-1}(r(t),\theta(t) - \varphi(t))\dot{\tilde{\omega}}(t) - \frac{\alpha}{\hat{\alpha}}RZ_e(t) \tag{27}$$
$$- \alpha(k_1\eta(t) + k_2\mathrm{sgn}(\eta(t))) - T^{-1}(r(t),\theta(t) - \varphi(t))[f(t)]$$
$$+ T^{-1}(r(t),\theta(t) - \varphi(t))\left[(\alpha\frac{\hat{\beta}}{\hat{\alpha}} - \beta)\omega^*(t) + \left(\frac{\alpha - \hat{\alpha}}{\hat{\alpha}}\right)\dot{\omega}^*(t)\right]$$
$$= -\beta\eta(t) - \alpha(k_1\eta(t) + k_2\mathrm{sgn}(\eta(t))) - \frac{\alpha}{\hat{\alpha}}RZ_e(t) - \left(\frac{\tilde{\alpha}}{\hat{\alpha}}\right)T^{-1}(r(t),\theta(t) - \varphi(t))\dot{\tilde{\omega}}(t)$$
$$- T^{-1}(r(t),\theta(t) - \varphi(t))[f(t)]$$
$$+ \alpha T^{-1}(r(t),\theta(t) - \varphi(t))\frac{\hat{\beta}}{\hat{\alpha}}\omega^*(t) - \tilde{\beta}T^{-1}(r(t),\theta(t) - \varphi(t))\omega^*(t)$$
$$+ \left(\frac{\tilde{\alpha}}{\hat{\alpha}}\right)T^{-1}(r(t),\theta(t) - \varphi(t))\dot{\omega}^*(t)$$

where $\tilde{\alpha} = \alpha - \hat{\alpha}$ and $\tilde{\beta} = \beta - \hat{\beta}$. The closed-loop stability and the parameter adjustment rules for $\hat{\alpha}$ and $\hat{\beta}$ can be simultaneously achieved by the Lyapunov stability theory. In doing so, one chooses the following radial and unbounded Lyapunov function candidate

$$V_3(t) = \frac{1}{2}Z_e^T(t)Z_e(t) + \frac{1}{2}\eta^T(t)\eta(t) + \frac{1}{2\lambda_\alpha}\tilde{\alpha}^2 + \frac{1}{2\lambda_\beta}\tilde{\beta}^2, \ \lambda_\alpha > 0, \ \lambda_\beta > 0 \tag{28}$$

which gives its time derivative along with the trajectories of Eq. 22 and 27

$$
\begin{aligned}
\dot{V}_3(t) = {}& Z_{\mathrm e}^{\mathrm T}\left(-K_{\mathrm p}Z_{\mathrm e}(t) + R\eta(t)\right) + \eta^T(t) \\
& \left\{ -\beta\eta(t) - \alpha(k_1\eta(t) + k_2\mathrm{sgn}(\eta(t))) - \tfrac{\alpha}{\hat\alpha}RZ_{\mathrm e}(t) - \left(\tfrac{\tilde\alpha}{\hat\alpha}\right)T^{-1}(r(t),\theta(t)-\varphi(t))\dot{\tilde\omega}(t) \right. \\
& -T^{-1}(r(t),\theta(t)-\varphi(t))[f(t)] + \tilde\alpha T^{-1}(r(t),\theta(t)-\varphi(t))\tfrac{\hat\beta}{\hat\alpha}\omega^*(t) - \tilde\beta T^{-1} \\
& \left. (r(t),\theta(t)-\varphi(t))\omega^*(t) + \left(\tfrac{\tilde\alpha}{\hat\alpha}\right)T^{-1}(\theta(t)-\varphi(t))\dot\omega^*(t)\right\} \\
& + \tfrac{1}{\lambda_\alpha}\left(-\tilde\alpha\dot{\hat\alpha}\right) + \tfrac{1}{\lambda_\beta}\left(-\tilde\beta\dot{\hat\beta}\right) \\
= {}& -Z_{\mathrm e}^{\mathrm T}K_{\mathrm p}Z_{\mathrm e}(t) - (\beta + \alpha k_1)\eta^T(t)\eta(t) - \alpha k_2\|\eta(t)\|_1 - \eta^T(t)T^{-1} \\
& (r(t),\theta(t)-\varphi(t))[f(t)] - \left(\tfrac{\tilde\alpha}{\hat\alpha}\right) \\
& \left[R\eta^T(t)Z_e(t) + \eta^T(t)T^{-1}(r(t),\theta(t)-\varphi(t))\dot{\tilde\omega}(t) \right. \\
& \left. -\hat\beta\eta^T(t)T^{-1}(r(t),\theta(t)-\varphi(t))\omega^*(t) - \eta^T(t)T^{-1}(r(t),\theta(t)-\varphi(t))\dot\omega^*(t)\right] \\
& -\eta^T(t)\tilde\beta T^{-1}(r(t),\theta(t)-\varphi(t))\omega^*(t) + \tfrac{1}{\lambda_\alpha}\left(-\tilde\alpha\dot{\hat\alpha}\right) + \tfrac{1}{\lambda_\beta}\left(-\tilde\beta\dot{\hat\beta}\right)
\end{aligned}
\tag{29}
$$

If the parameter adjustment rules for $\hat\alpha$ and $\hat\beta$ are selected such that

$$
\begin{aligned}
& \tfrac{1}{\hat\alpha}\left[R\eta^{\mathrm T}(t)Z_{\mathrm e}(t) + \eta^{\mathrm T}(t)T^{-1}(r(t),\theta(t)-\varphi(t))\dot{\tilde\omega}(t) - \hat\beta\eta^{\mathrm T}(t)T^{-1} \right. \\
& \left. (r(t),\theta(t)-\varphi(t))\omega^*(t) - \eta^{\mathrm T}(t)T^{-1}(r(t),\theta(t)-\varphi(t))\dot\omega^*(t)\right] \\
& + \tfrac{1}{\lambda_\alpha}\left(\dot{\hat\alpha}\right) = 0
\end{aligned}
\tag{30}
$$

and

$$
\eta^{\mathrm T}(t)T^{-1}(r(t),\theta(t)-\varphi(t))\omega^*(t) + \tfrac{1}{\lambda_\beta}\left(\dot{\hat\beta}\right) = 0
\tag{31}
$$

then

$$
\begin{aligned}
\dot{V}_3(t) = {}& -Z_{\mathrm e}^{\mathrm T}K_{\mathrm p}Z_{\mathrm e}(t) - (\beta + \alpha k_1)\eta^{\mathrm T}(t)\eta(t) \\
& - \alpha k_2\|\eta(t)\|_1 - \eta^{\mathrm T}(t)T^{-1}(r(t),\theta(t)-\varphi(t))[f(t)] \\
\leq {}& -Z_e^{\mathrm T}K_pZ_e(t) - (\beta + \alpha k_1)\eta^T(t)\eta(t) \\
& - \alpha k_2\|\eta(t)\|_1 + \|\eta(t)\|_1\big\|T^{-1}(r(t),\theta(t)-\varphi(t))f(t)\big\|_\infty \\
\leq {}& -Z_{\mathrm e}^{\mathrm T}K_pZ_{\mathrm e}(t) - (\beta + \alpha k_1)\eta^{\mathrm T}(t)\eta(t) - \alpha\left(k_2 - \tfrac{k_{\max}}{\alpha}\right)\|\eta(t)\|_1 < 0
\end{aligned}
\tag{32}
$$

which reveals that $\dot{V}_3(t)$ is negative semidefinite and $V_3(t)$ is indeed a Lyapunov function. The use of the LaSalle's invariance principle implies that $Z_{\mathrm e}\to 0$ and $\eta\to 0$ as time tends to

infinity, and the estimates $\widehat{\alpha}$ and $\widehat{\beta}$ are globally uniformly bounded. Similarly, $\eta(t) \to 0$ as $t \to \infty$ indicates that $\widetilde{\omega}(t) \to 0$ as $t \to \infty$. Moreover, from Eqs. 30 and 31 one obtains the parameter adjustment rules for $\widehat{\alpha}$ and $\widehat{\beta}$

$$
\dot{\widehat{\alpha}} = -\lambda_\alpha \frac{1}{\widehat{\alpha}} [R\eta^{\mathrm{T}}(t)Z_{\mathrm{e}}(t) + \eta^{\mathrm{T}}(t)T^{-1}(r(t),\theta(t) - \varphi(t))\widetilde{\omega}(t) \tag{33}
$$
$$
- \widehat{\beta}\eta^{\mathrm{T}}(t)T^{-1}(r(t),\theta(t) - \varphi(t))\omega^*(t) - \eta^T(t)T^{-1}(r(t),\theta(t) - \varphi(t))\dot{\omega}^*(t)]
$$

and

$$
\dot{\widehat{\beta}} = -\lambda_\beta \eta^T(t)T^{-1}(r(t),\theta(t) - \varphi(t))\omega^*(t) \tag{34}
$$

The following theorem summarizes the aforementioned result.

Theorem 2 *Consider the platform's kinematic model (8) along with the motors' dynamic model (11) where the two parameters α and β are unknown but constant. If the adaptive controller (Eq. 26) with the parameter adjustment rules 33 and 34 are applied, then the platform can be steered to reach any destination pose or exactly follow any differentiable and time-varying trajectory, $Z_{\mathrm{d}}(t) = [r_{\mathrm{d}}(t) \quad \varphi_{\mathrm{d}}(t) \quad \theta_{\mathrm{d}}(t)]^T \in C^1$, in the sense of globally exponential stability, i.e., $r(t) \to r_{\mathrm{d}}(t)$, $\varphi(t) \to \varphi_{\mathrm{d}}(t)$, and $\theta(t) \to \theta_{\mathrm{d}}(t)$ as $t \to \infty$.*

4 Adaptive Robust Path Following Control

This section is dedicated to addressing the path following control problem of the platform in polar coordinates. As mentioned before, the trajectory tracking problem is formulated in tracking a virtual reference at a given velocity, namely that the reference curve is some function of time. However, in many applications, it is not necessary for the omnidirectional mobile platforms to obtain certain postures at specified instants. Hence, path following is of practical significance to accurately follow the geometric path. In the following we attempt to deal with the path following problem under the assumption of desired linear velocity. To achieve the control goal, the desired path to be followed is first described, and the path following controller is then synthesized. Let the polar radius of the reference path be a C^2 function of the polar angle, namely that

$$
r_{\mathrm{d}} = f(\varphi_{\mathrm{d}}) \tag{35}
$$

which gives

$$
\dot{r}_{\mathrm{d}}(t) = \frac{\mathrm{d}r_{\mathrm{d}}}{\mathrm{d}t} = r_{\mathrm{d}}'(\varphi_{\mathrm{d}})\dot{\varphi}_{\mathrm{d}}(t) \tag{36}
$$

and

$$
\ddot{r}_{\mathrm{d}}(t) = \frac{\mathrm{d}^2 r_{\mathrm{d}}}{\mathrm{d}^2 t} = r_{\mathrm{d}}''(\varphi_{\mathrm{d}}(t))\dot{\varphi}_{\mathrm{d}}^2(t) + r_{\mathrm{d}}'(\varphi_{\mathrm{d}}(t))\ddot{\varphi}_{\mathrm{d}}(t) \tag{37}
$$

where $r_d'(\varphi_d) = \frac{dr_d(\varphi_d)}{d\varphi_d}$; $r_d''(\varphi_d) = \frac{d^2 r_d(\varphi_d)}{d^2 \varphi_d}$; $\dot{\varphi}_d(t)$ and $\ddot{\varphi}_d(t)$ are determined as follows. With Eq. 4 and the desired linear velocity $v_d(t)$ of the platform give

$$\left(\dot{r}_d(t)\right)^2 + \left(r_d(\varphi_d)\dot{\varphi}_d(t)\right)^2 = v_d^2(t) \tag{38}$$

Since $\dot{r}_d(t) = r_d'(\varphi_d)\dot{\varphi}_d(t)$, Eq. 38 becomes

$$\left(r_d'(\varphi_d)\dot{\varphi}_d(t)\right)^2 + \left(r_d(\varphi_d)\dot{\varphi}_d(t)\right)^2 = v_d^2(t) \tag{39}$$

Solving for the variable $\dot{\varphi}_d(t)$ from Eq. 39 yields

$$\dot{\varphi}_d(t) = \frac{v_d(t)}{\sqrt{r_d^2(\varphi_d) + r_d'^2(\varphi_d)}} \tag{40}$$

Notice that the positive sign is preferred in Eq. 40, and the desired linear velocity $v_d(t)$ can be designated as negative. Moreover, differentiating Eq. 40 with respect to time yields

$$\ddot{\varphi}_d(t) = -\frac{r_d'(\varphi_d(t))\left(r_d''(\varphi_d(t)) + r_d(\varphi_d(t))\right)\dot{\varphi}_d^2(t)}{\left(r_d^2(\varphi_d(t)) + r_d'^2(\varphi_d(t))\right)} \tag{41}$$

Hence, Eqs. 40 and 41 define the motion of the parameter $\varphi_d(t)$.

Furthermore, the tangential angle of the reference path (35) in polar coordinates is obtained from

$$\theta_d(t) = {}^\pi\!/_2 + \varphi_d(t) - \tan^{-1}\left(r_d'(\varphi_d)\big/ r_d(\varphi_d)\right) \tag{42}$$

which has its time derivative

$$\begin{aligned}
\dot{\theta}_d(t) &= \dot{\varphi}_d(t) - \frac{r_d(\varphi_d)r_d''(\varphi_d)\dot{\varphi}_d(t) - \left(r_d'(\varphi_d)\right)^2\dot{\varphi}_d(t)}{r_d^2(\varphi_d) + \left(r_d'(\varphi_d)\right)^2} \\
&= \dot{\varphi}_d(t)\left(\frac{2\left(r_d'(\varphi_d)\right)^2 + r_d^2(\varphi_d) - r_d(\varphi_d)r_d''(\varphi_d)}{r_d^2(\varphi_d) + \left(r_d'(\varphi_d)\right)^2}\right)
\end{aligned} \tag{43}$$

Unlike the conventional two-wheeled mobile platforms, the desired vehicle's orientation $\theta_d(t)$ for the omnidirectional mobile platform can not be necessary to be the tangential angle of the reference path, but can be arbitrarily planned. Once the desired path (Eq. 35) and the given orientation and their first and second time derivatives 36, 37, 40 and 41 have been obtained, the path following controller will be synthesized such that the platform will follow the desired path in the sense of globally asymptotical stability, i.e., $r(t) \rightarrow r_d(t)$, $\varphi(t) \rightarrow \varphi_d(t)$, $\theta(t) \rightarrow \theta_d(t)$ as $t \rightarrow \infty$. The work can be done easily by proceeding with the previous design procedure as in Section 3. To achieve the controller design for the platform's kinematic model (8) along with the motors' dynamic model (11) with unknown but constant parameters, α and β, as well as three uncertain but bounded forces, f_i, $i=1, 2, 3$, exerted on the driving wheels, we use the tracking error vector as in Eq. 12 and the adaptive robust controller (Eq. 26) with the parameter adjustment rules (Eq. 33) and (Eq. 34). Then the following theorem is given.

Theorem 3 *Consider the platform's kinematic model (8) and the motors' dynamic model (11) with the desired path (Eq. 35). If the adaptive robust controller (Eq. 26) with the parameter adjustment rules (Eq. 33) and (Eq. 34) are employed and the polar radius is always nonzero and bounded, then the platform can be steered to exactly follow the path in the sense of globally asymptotical stability.*

Remark 1 The linear velocity $v_d(t)$ of the platform can be designated by the user according to the curvature of the path (Eq. 35), in order to avoid the generation of the large transient tracking error. For example, if the curvature is small, then the linear velocity $v_d(t)$ becomes fast; if the curvature is large, then the linear velocity $v_d(t)$ becomes slow. Simple fuzzy rules with genetic algorithm might be useful in finding appropriate linear velocity $v_d(t)$ for the platform to follow a given path.

Remark 2 Although the current trajectory generator for path following assumes linear velocity, it is possible to generate energy-optimal or time-optimal trajectories [12, 17] for the kind of vehicle.

5 Simulation Results

The aim of the simulations is to examine the effectiveness and performance of the proposed control methods. These simulations were conducted with the following parameters: $L=$ 0.23 m, $R=0.0508$ m, $\alpha=\beta=0.4$, $k_1=k_2=3$, $\lambda_\alpha = \lambda_\beta = 2$, $f_1=f_2=f_3=0.3$ (N), and $K_p=$diag $\{7.5, 7.5, 7.5\}$.

5.1 Adaptive Robust Trajectory Tracking of Rose Curves

The following two simulations were used to study the performance of the adaptive robust control law (Eq. 26) by tracking the special rose curves expressed by $r_d(t) = 5\cos\left(\frac{1}{3}\varphi_d(t)\right) + 6$ (unit:m) and $r_d(t) = 5\cos(4\varphi_d(t)) + 8$ (unit:m). The initial pose of the omnidirectional mobile platform was assumed at $[r_0 \quad \varphi_0 \quad \theta_0]^T = [1\text{m} \ 0 \text{ rad} \quad 0 \text{ rad}]^T$ and the desired vehicle orientation was $\pi/2$. Figure 2(a) depicts the tracking performance of the controlled platform to track the rose curve $r_d(t) = 5\cos\left(\frac{1}{3}\varphi_d(t)\right) + 6$, and Fig. 2(b) presents the simulated trajectory tracking of rose curve $r_d(t) = 5\cos(4\varphi_d(t)) + 8$. The convergent tracking errors of position and orientation for rose curve described in Fig. 2(a) are shown in Fig. 3. The results clearly reveal that the control law (Eq. 26) was capable of steering the platform to track these special paths.

The third simulation for tracking rose curve trajectory was conducted to compare the proposed adaptive robust controller (Eq. 26) with the non-adaptive robust controller (Eq. 20). The two parameters $\alpha=\beta=0.4$ are again used to perform the simulation for $0 \leq t \leq 80$ s., but they are altered to $\alpha=\beta=0.41$ in the time interval 30 $s \leq t \leq 35$ s. Figure 4 presents the trajectory tracking performance of the non-adaptive robust controller (Eq. 20). Comparing Fig. 4 with Fig. 2(a), the adaptive robust controller has a more smooth response to track the rose curve than the non-adaptive one does, especially in the time interval $30\,s \leq t \leq 35\,s$. This result clearly indicates that the proposed adaptive robust controller (Eq. 26) outperforms the non-adaptive roust one (Eq. 20).

Fig. 2 Simulation results of the proposed adaptive controller for tracking rose curves. **a** $r_d(t) = 5 \cos\left(\frac{1}{3} \varphi_d(t)\right) + 6$. **b** $r_d(t) = 5 \cos\left(4 \varphi_d(t)\right) + 8$


a

b
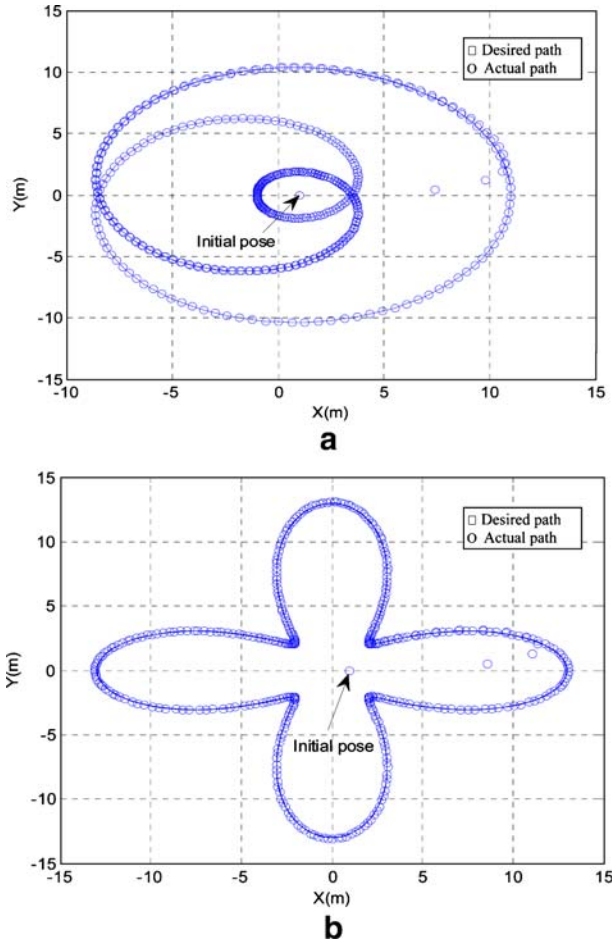
5.2 Adaptive Robust Path Following

The objective of the subsequent path following simulation is to investigate how the adaptive robust control law (Eq. 26) along with the parameter adjustment rules (Eq. 33) and (Eq. 34) can be applied to achieve the path following mission. The first illustrative simulation was performed to steer the platform to follow the special path, called Limacon of Pascal, expressed by

$$r_d(t) = 15 + 10 \cos \varphi_d(t) \quad (\text{Unit}:\text{m})$$

where $\varphi_d(t)$ is assumed to be 0.3 rad.; thus, the desired velocity of the platform was obtained from Eq. 40, i.e., $v_d(t) = \sqrt{29.25 + 27 \cos (\varphi_d(t))}$ m/s.; the desired vehicle orientation was $\pi/2$; the initial pose of the platform was given by $\begin{bmatrix} r_0 & \varphi_0 & \theta_0 \end{bmatrix}^T = \begin{bmatrix} 1\text{m} & 0\text{ rad} & 0\text{ rad} \end{bmatrix}^T$. Figure 5(a) shows the simulation response for the special path. Figure 5(b) shows the convergent errors of position and orientation. The result indicates that the controller (Eq. 26) was capable of steering the platform to follow this special path.

a

b

c
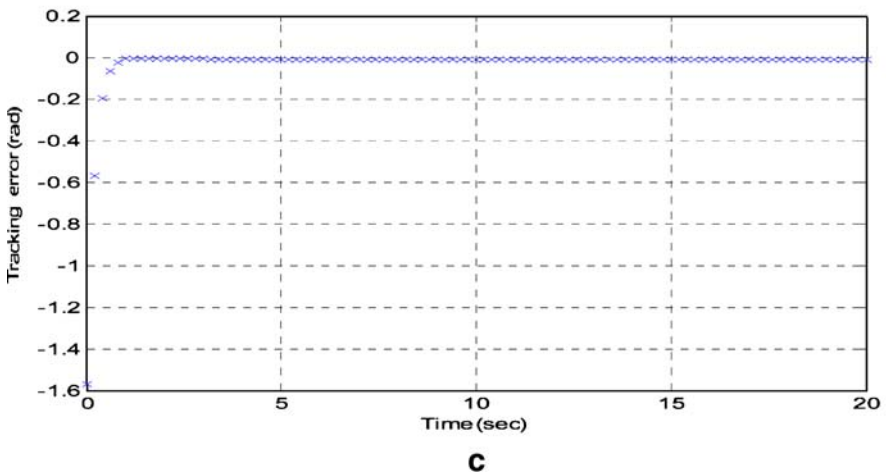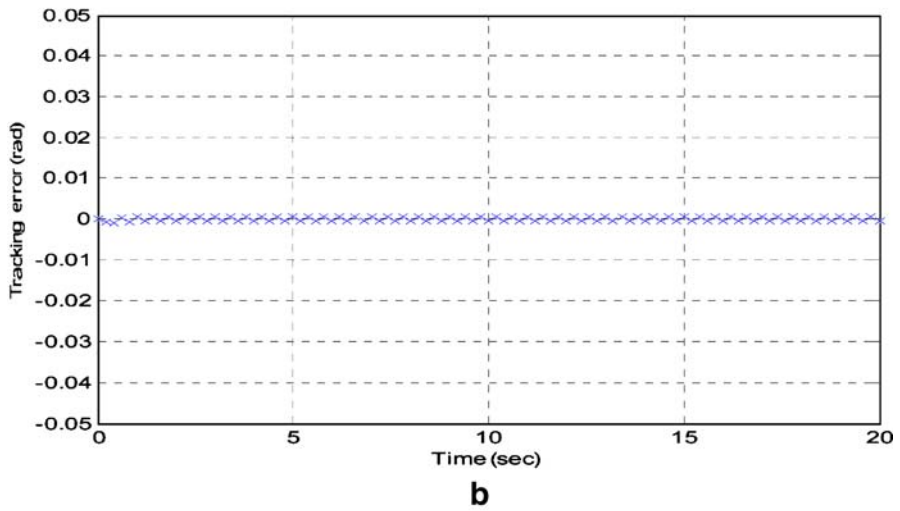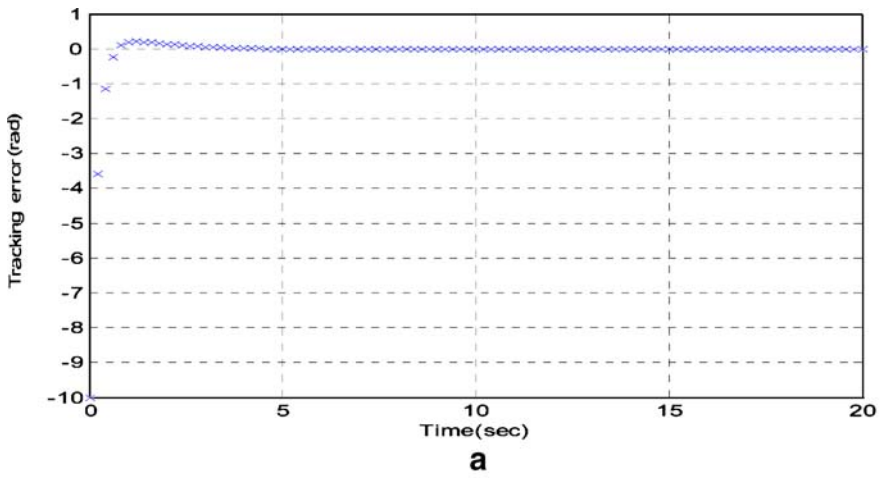
Fig. 3 Trajectory tracking performance of the proposed adaptive controller for rose curve in Fig. 2(a). **a** Convergent tracking error of r. **b** Convergent tracking error of φ. **c** Convergent tracking error of θ

Furthermore, the second simulation conducted the simulation of Limacon of Pascal path following problem in Cartesian coordinates, and then compared the result with the previous one in polar coordinates. An existing path-tracking controller proposed in [19] was adopted to perform the simulation. Figure 6 depicts the path following simulation result of the Limacon of Pascal in Cartesian coordinates. Comparing Fig. 6 with Fig. 5(a), the polar-space adaptive controller (Eq. 26) exhibits a much smoother trajectory and less path following errors, thus showing the merit of the adaptive controller in following smooth trajectories expressed in polar-coordinates.

6 Experimental Results and Discussion

The aim of the following experiments is to examine the effectiveness and performance of the proposed adaptive robust control method. As shown in Fig. 7, the experimental omnidirectional mobile robot is equipped with the following components: (1) one 7" LCD monitor; (2) one personal computer (PC); (3) three encoders mounted on the driving motors; (4) two 12 V serial batteries; (5) three DC24V brushless servomotors with their drivers from Oriental Motor Co., Taiwan; (6) three omnidirectional wheels from Kornylak Corporation (Kornylak.com); (7) one five-link robot arm; (8) one laser scanner. The personal computer is composed of a one parallel digital input and output circuit card with three 32-bit counters HCTL2032, and one digital-to-analog card (PIO-DA9). Three driving omnidirectional wheels are driven by three DC24V brushless servomotors with three mounted encoders of 300 pulses per revolution. The proposed unified control law (Eq. 26) was implemented using C++ codes and standard programming techniques. All the experiments were conducted with the system parameters: $L=23$ cm and $R=5.08$ cm.

Moreover, in the experiments, the three encoders were employed to measure the angular velocities of the three DC brushless motors in order to achieve the dead-reckoning of the platform. The purpose of the dead-reckoning of the platform is, given a correct initial pose,

Fig. 4 Trajectory tracking performance for rose curve $r_d(t) = 5\cos\left(\frac{1}{3}\varphi_d(t)\right) + 6$ using the non-adaptive robust controller (Eq. 20)
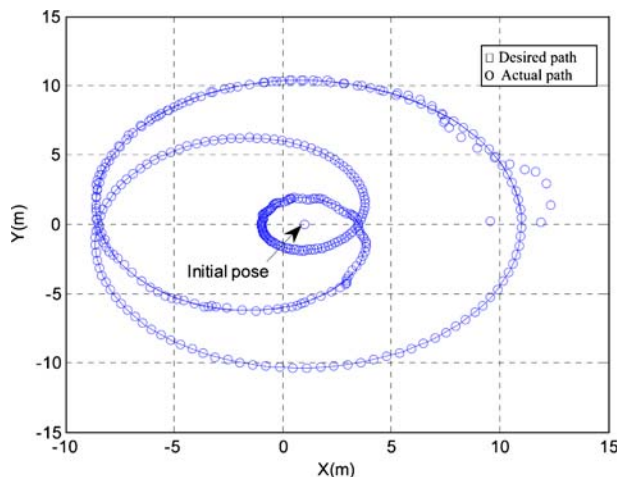
Fig. 5 **a** Path following result for the Limacon of Pascal $r_d(t) = 15 + 10 \cos \varphi_d(t)$. **b** Path following errors of the proposed adaptive controller in Fig. 5(a)
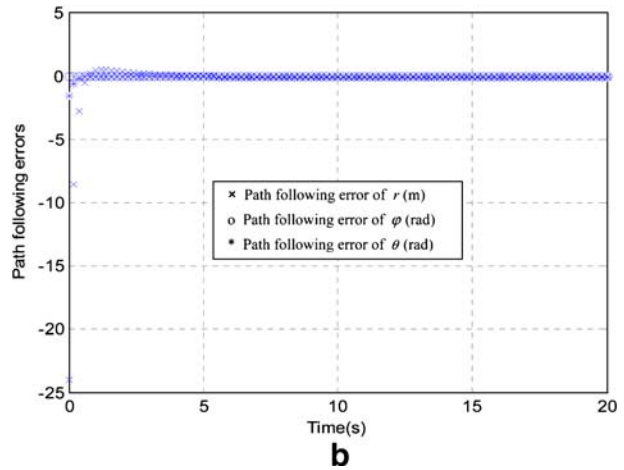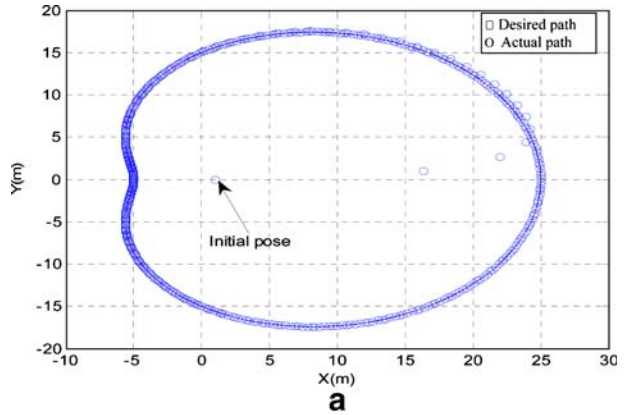

a

b

Fig. 6 Path following result for the Limacon of Pascal $r_d(t) = 15 + 10 \cos \varphi_d(t)$ using the controller proposed by [19] in Cartesian coordinates
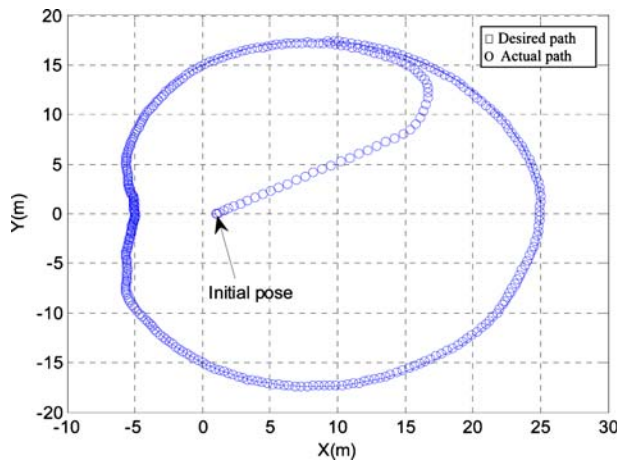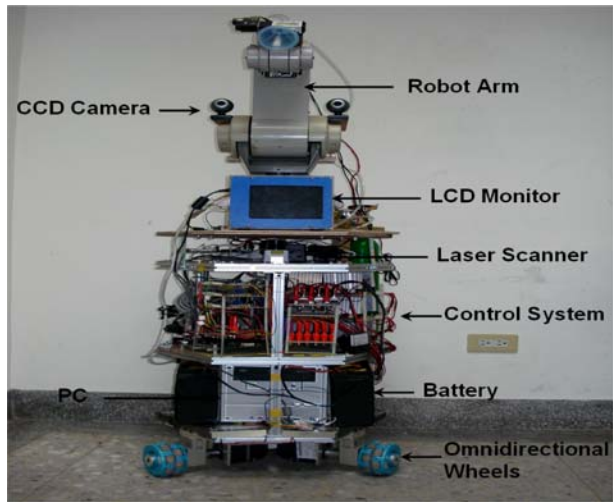
Fig. 7 Picture of the experimental omnidirectional mobile robot

to continuously keep track of its correct poses with respect to the reference frame. This dead-reckoning pose estimation can be improved by fusing laser scanning data.

6.1 Elliptical Trajectory Tracking

The elliptic trajectory tracking experiment was employed to explore how the proposed controller (Eq. 26) steers the mobile platform to exactly follow an elliptic trajectory described by

$$
\begin{pmatrix} r_{\mathrm{d}}(t) & \varphi_{\mathrm{d}}(t) & \theta_{\mathrm{d}}(t) \end{pmatrix} = \begin{pmatrix} \dfrac{1}{\sqrt{\frac{1}{2r_1^2} + \frac{1}{2r_2^2} + \cos\left(2\,\varphi_{\mathrm{d}}(t)\right)\left(\frac{1}{2r_1^2} - \frac{1}{2r_2^2}\right)}} & \omega_{\mathrm{o}} + \omega_r t & \dfrac{\pi}{2} \end{pmatrix}
$$

The experiment assumed that the platform got started at $\begin{bmatrix} r_0 & \varphi_0 & \theta_0 \end{bmatrix}^T = \begin{bmatrix} 1.0 \text{ cm} \\ 0.0 \text{ rad} & 0.0 \text{ rad} \end{bmatrix}$. The parameters in the elliptic trajectory tracking experiment were taken as follows: $\omega_0 = 0$ (rad/s), $\omega_r = 0.2$ (rad/s), $r_1 = 20$ (cm), $r_2 = 30$ (cm). Figure 8(a) depicts the experimental elliptic trajectory tracking of the platform. The tracking errors for elliptical trajectory are shown in Fig. 8(b). These results show that the polar-space adaptive robust controller (Eq. 26) is capable of steering the omnidirectional mobile platform to exactly track the elliptic trajectory.

6.2 Limacon of Pascal Path Following Experiment

The objective of the subsequent experiment is to examine and verify the effectiveness of the proposed unified control law (Eq. 26) for path following. The illustrative experiment was performed to steer the platform to follow the special path, called Limacon of Pascal, expressed by

$$
r_{\mathrm{d}}(t) = 20 + 15 \cos \varphi_{\mathrm{d}}(t) \quad (\text{unit} : \text{cm})
$$

where $\dot{\varphi}_{\mathrm{d}}(t)$ is assumed to be 0.1 rad.; thus, the desired velocity of the platform was obtained from (Eq. 40), i.e., $v_{\mathrm{d}}(t) = \sqrt{6.25 + 6 \cos\left(\varphi_{\mathrm{d}}(t)\right)}$ cm/s.; the desired vehicle

Fig. 8 **a** Experimental result of
the elliptic trajectory tracking. **b**
Experimental tracking errors of
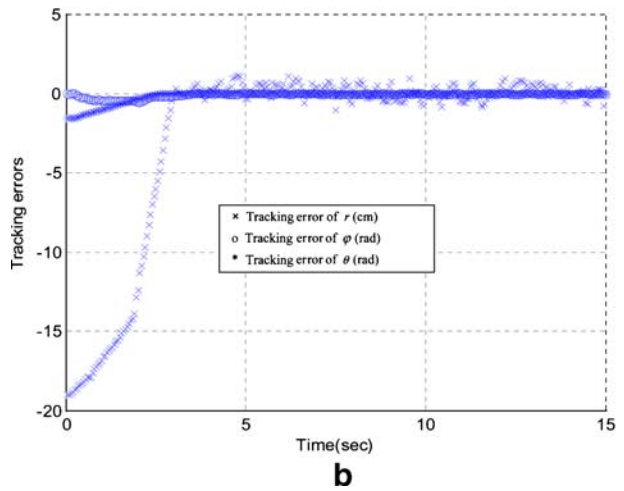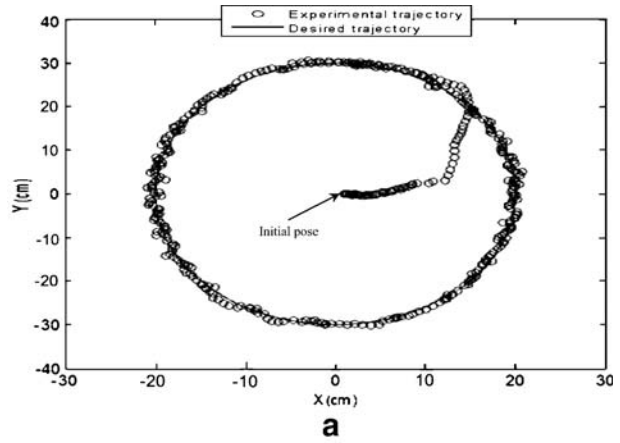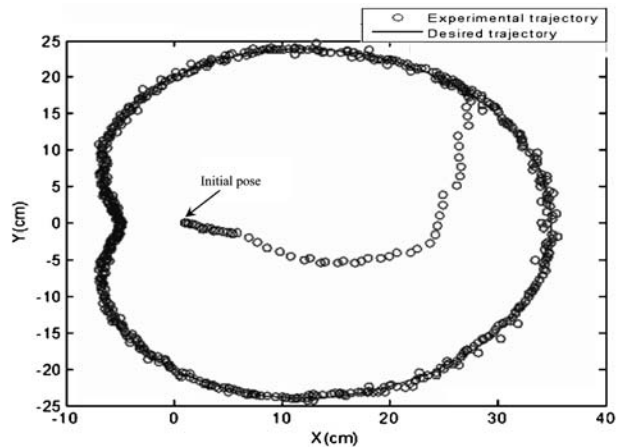the elliptic trajectory in
Fig. 8(a)

a

b

Fig. 9 Experimental result of the
Limacon of Pascal
$r_d(t) = 20 + 15 \cos \varphi_d(t)$ path
following

orientation was $\pi/2$; the initial pose of the platform was given by $[r_0 \ \varphi_0 \ \theta_0]$=[1.0 cm 0 rad 0 rad]. Figure 9 depicts the experiment result of the Limacon of Pascal path following. The result shows that the adaptive robust controller (Eq. 26) in polar-coordinates is capable of steering the platform to follow this desired path.

7 Conclusions

This paper has developed an adaptive robust control method via backstepping for trajectory tracking and path following of an omnidirectional mobile platform with two actuators' uncertainties. With the platform's wheels equally spaced at 120° from one another, the polar-space kinematic model of the platform is briefly described, and the simplified dynamic equations of the three DC servomotors with two unknown parameters are also given. The adaptive robust controller has been designed in two steps. The robust controller is first presented and the adaptive one is then constructed in order to achieve trajectory tracking. The adaptive robust control method has been easily applied to address the path following problem for the platform in polar coordinates. Through computer simulation and experimental results, the proposed controllers have been shown capable of steering the platform to achieve the tasks or missions of trajectory tracking and path following in polar coordinates; furthermore, it outperforms the non-adaptive robust controller and the feedback controller shown in [19].

References

1. Aicardi, M., Caslino, G., Bicchi, A., Balestrino, A.: Closed loop steering of unicycle-like vehicles via Lyapunov techniques. IEEE Robot. Autom. Mag. 2, (1), 27–35 (1995)
2. Behal, A., Dawson, D.M., Dixon, W.E., Fang, Y.: Robust tracking and regulation control for mobile robots. IEEE Proc. Conf. Control Appl, Kohala Coast-Island of Hawai'i, Hawai'i, USA, August 22–27, 1015–1020 (1999)
3. Carter, B., Good, M., Dorohoff, M., Lew, J., Williams, R.L., Gallina, P.: Mechanical design and modeling of an omni-directional robocup player. Proceedings of RoboCup 2001 International Symposium, Seattle, WA, USA, August, (2001)
4. Chwa, D.K.: Sliding mode tracking control of nonholonomic wheeled mobile robots in polar coordinates. IEEE Trans. Control Syst. Technol. 12, (4), 637–644 (2004)
5. Dixon, W.E., Dawson, D.M., Zergeroglu, E., Zhang, F.: Robust tracking and regulation control for mobile robots. Int. J. Robust Nonlinear Control. 10, 199–216 (2000)
6. Do, K.D., Jiang, Z.P., Pan, J.: A global output-feedback controller for simultaneous tracking and stabilization of unicycle-type mobile robots. IEEE Trans. Robot Autom. 20, (3), 589–594 (2004)
7. Do, K.D., Jiang, Z.P., Pan, J.: Simultaneous tracking and stabilization of mobile robots: an adaptive approach. IEEE Trans. Automat. Contr. 49, (7), 1147–1151 (2004)
8. Driessen, B.J.: Adaptive global tracking for robots with unknown link and actuator dynamics. Int. J. Adapt. Control Signal Process. 20, 123–38 (2006)
9. Jiang, Z.P., Nijmeijer, H.: Tracking control of mobile robots: a case study in backstepping. Automatica. 33, 1393–1399 (1997)
10. Jiang, Z.P., Nijmeijer, H.: A recursive technique for tracking control of nonholonomic systems in chained form. IEEE Trans. Automat. Contr. 44, 265–279 (1999)
11. Jung, M.J., Kim, H.S., Kim, S., Kim, J.H.: Omni-directional mobile base OK-II. Proceeding of the IEEE Int. Conf. Robot. Autom. 3449–3454 (2000)

12. Kalmár-Nagy, T., D'andrea, R., Ganguly, P.: Near-optimal dynamic trajectory generation and control of an omnidirectional vehicle.. Robot. Autono. Syst. 46, 47–64 (2004)
13. Khalil, H.K.: Nonlinear Systems, 3rd Ed.rd edn. Prentice Hall, Upper Saddle, NJ (2002)
14. Lee, T.C., Song, K.T., Lee, C.H., Teng, C.C.: Tracking control of unicycle-modeled mobile robots using a saturation feedback controller. IEEE Trans. Control Syst. Technol. 9, 305–318 (2001)
15. Park, K., Chung, H., Lee, J.G.: Point stabilization of mobile robots via state-space exact feedback linearization. Robot. Comp.-Integr. Manuf. 16, (5), 353–363 (2000)
16. Pin, F.G., Killough, S.M.: A new family of omnidirectional and holonomic wheeled platforms for mobile robots. IEEE Trans. Robot Autom 10, (4), 480–489 (1994)
17. Red, E.: A dynamic optimal trajectory generator for Cartesian path following. Robotica. 18, 451–458 (2000)
18. Tsai, C.C., Wang, T.S.: Nonlinear control of an omnidirectional mobile robot. Proc. 8th Intl. Conf. Autom Technol. 727–732 (2005)
19. Watanabe, K., Shiraishi, Y., Tzafestas, S., Tang, J., Fukuda, T.: Feedback control of an omnidirectional autonomous platform for mobile service robots. J. Intell. Robot. Syst. 22, 315–330 (1998)
20. Williams II, R.L., Carter, B.E., Gallina, P., Rosati, G.: Dynamic model with slip for wheeled omnidirectional robots. IEEE Trans. Robot. Autom. 18, (3), 285–293 (2002)
21. Wu, C.J., Tsai, C.C.: Localization of an autonomous mobile robot based on ultrasonic sensory information. J. Intell. Robot. Syst. 30, 267–277 (2001)
22. Yang, J.M., Kim, J.H.: Sliding mode control for trajectory tracking of nonholonomic wheeled mobile robots. IEEE Trans. Robot. Automa. 15, (3), 578–587 (1999)
23. Yang, Z., Red, E.: On-line Cartesian trajectory control of mechanism along complex curves. Robotica. 15, 263–274 (1997)